ORIGINAL RESEARCH

Silver Citrate Nanoparticles Inhibit PMA-Induced TNFα Expression via Deactivation of NF-κB Activity in Human Cancer Cell-Lines, MCF-7

Ahmed AH Abdellatif [1,2]
Zafar Rasheed [3]
Ahmad H Alhowail [4]
Abdulmajeed Alqasoumi [5]
Mansour Alsharidah [6]
Riaz A Khan [7]
Abdullah SM Aljohani [8]
Maha A Aldubayan [4]
Waleed Faisal [9,10]

[1]Department of Pharmaceutics, College of Pharmacy, Qassim University, Buraydah 51452, Kingdom of Saudi Arabia; [2]Department of Pharmaceutics and Industrial Pharmacy, Faculty of Pharmacy, Al-Azhar University, Assiut 71524, Egypt; [3]Department of Medical Biochemistry, College of Medicine, Qassim University, Buraydah 51452, Kingdom of Saudi Arabia; [4]Department of Pharmacology and Toxicology, College of Pharmacy, Qassim University, Buraydah 51452, Kingdom of Saudi Arabia; [5]Department of Pharmacy Practice, College of Pharmacy, Qassim University, Buraydah 51452, Kingdom of Saudi Arabia; [6]Department of Physiology, College of Medicine, Qassim University, Buraydah 51452, Kingdom of Saudi Arabia; [7]Department of Medicinal Chemistry and Pharmacognosy, College of Pharmacy, Qassim University, Buraydah 51452, Kingdom of Saudi Arabia; [8]Department of Veterinary Medicine, College of Agriculture and Veterinary Medicine, Qassim University, Buraydah, Kingdom of Saudi Arabia; [9]School of Pharmacy, University College Cork, Cork, Ireland; [10]Faculty of Pharmacy, Minya University, Minya, Egypt

Correspondence: Ahmed AH Abdellatif
College of Pharmacy, Qassim University, Buraydah 51452, Kingdom of Saudi Arabia
Email a.abdellatif@qu.edu.sa

Background: The nuclear factor kappa-B (NF-κB) is a major transcription factor responsible for the production of numerous inflammatory mediators, including the tumor necrosis factor (TNFα), which has a lethal association with cancer's onset. The silver nanoparticles (AgNPs) are widely used in cancer treatment and several other biomedical applications.

Objective: The study aimed to determine the effects of silver citrate nanoparticles (AgNPs-CIT) on NF-κB activation together with TNFα mRNA/protein expressions in the phorbol myristate acetate (PMA)-stimulated MCF-7 human breast cancer cell-lines.

Methods: The AgNPs-CIT were synthesized by the reduction method, and the prepared AgNPs-CIT were characterized for their shape, absorption in UV-VIS electromagnetic radiations, size distribution, ζ-potential, and antioxidant activity. The MCF-7 cell-lines were pretreated with AgNPs-CIT and stimulated with PMA. The TNFα mRNA expressions were determined by real-time PCR, whereas the protein production was determined by the ELISA. The NF-κB activity was distinctly observed by highly-specific DNA-based ELISA, and by NF-κB-specific inhibitor, Bay 11–7082.

Results: The prepared AgNPs-CIT were spherical and have an absorption wavelength range of 381–452 nm wherein the particles size ranged between 19.2±0.1 to 220.77±0.12 nm with the charge range −9.99±0.8 to −34.63±0.1 mV. The prepared AgNPs-CIT showed comparative antioxidant activity at >40% inhibitions level of the DPPH radicals. The AgNPs-CIT were found to be non-toxic to MCF-7 cell-

lines and inhibited PMA-induced activation of the NF-κBp65, and also the mRNA/protein expression of TNFα.

Conclusion: This is the first report that showed AgNPs-CIT inhibited TNFα expression via deactivation of the NF-κB signaling event in stimulated breast cancer cells. The results have important implications for the development of novel therapeutic strategies for the prevention/treatment of cancers and/or inflammatory disorders.

Keywords: phorbol myristate acetate, PMA, TNFα, NF-κB, silver citrate nanoparticles, MCF-7 cell lines, cancer, inflammatory cytokines

Introduction

The advent of silver nanoparticles (AgNPs) in cancer theranostics has been unprecedented in the last two decades. The cancer nanomedicine has primarily been derived by the gold and silver nanostructures, whereby silver metal-based capped biogenic, and redox-methods based nano-entities preparations, and their applications in various oncogenic chemotherapeutic interventions have provided the needed impetus to the

silver nanoparticles as the leading nanomedicine part of the cancer chemotherapy.[1] The use of AgNPs has also been preferred on account of its ease availability, cost-effective preparation, and compatible toxicological behavior. AgNPs of different sizes, capping, charge, polydispersity index (PDI), and yields-density have been prepared through various biogenic, chemical as well as other in situ, and physical approaches.[2] The necessity and advancements of AgNPs preparation and capping variations have opened up newer vistas in cancer treatment. The genomic and proteomic supported changes in various aspects of oxidative stress controls in cancerous cells.[3]

Studies on cellular and systemic toxicity were undertaken, and it is reported that the AgNPs-CIT is not harmful, and are not considered toxic within cells.[4] Further, studies also demonstrated that the AgNPs-CIT can inhibit the PMA (phorbol 12-myristate 13-acetate) in monocytes through down-regulating both the expression of surface marker CD11b and reaction to lipopolysaccharide (LPS) stimulation.[5] The AgNPs-CIT has also has been shown to possess antitumor properties for Dalton's lymphoma ascites (DLA), both *in vitro* and *in vivo* conditions by activation of the caspase-3 enzyme, which led to curative effects in the tumor-borne mice by decreasing the weight and tumor volume.[6] More functional details and applications feasibility studies of these AgNPs genre have lately been appearing. In this connection, to deal with tumor suppression through various biochemical and physiological processes and conditions, the role of the tumor necrosis factor-alpha has also been judged crucial wherein the tumor necrosis factor-alpha (TNFα), a cytokine, generates acute stage reaction and is produced mainly by the stimulation of the macrophages, although it can also be generated by several other cell forms, eg, CD4+ lymphocytes, mast cells, neutrophils, eosinophils, and the neurons.[7]

The primary function of the TNFα is to control the immune cells. The TNFα is an endogenous pyrogen, and is capable of causing fever, cell-death through apoptosis, autonomic dysfunctions, inflammation, and inhibition of tumorigenesis, as well as viral replications, and reacting to sepsis through IL1 and IL6 producing cells. The TNFα output dysregulation has been implicated in several human diseases, including neurodegenerative disorders, including Alzheimer's disease.[8] It can also cause major depression,[7] several types of cancers,[9] and inflammatory bowel disease, owing to the increased levels of TNFα.[10] The TNFα also has a role in lethal septic shock and is recognized for the therapeutic effects of the monoclonal anti-TNF antibodies.[11]

The TNFα can also stop the death/apoptosis of neuronal cells by activating the transcription factor, NF-kappa-B, which causes the expressions of Mn-SOD (Mn-Super Oxide Dismutase), and Bcl-2.[12] It has been reported that the TNFα is elevated in the blood serum of patients with cancer physiology. The TNFα has also been associated with several metastases, eg, breast cancer,[13] non-small cell lung cancer (NSCLC),[14] colon cancer,[15] and leukemic cells.[16] Moreover, the high levels of TNFα were observed owing to the activation of NF-κB,[17] which has an established and critical role in the inflammation, and carcinogenesis.[18] A significant relationship between the expressions of the TNFα and the putative TNFα inducible NF-κB related genes in human breast cancer was found.[19] Ben-Baruch, 2003, found that the positive TNFα expression rate is related to that of the presence of NF-κB in the MCF-7 cell-lines.[20]

The PMA is a potent tumor promoter and is frequently used to activate the signal transduction enzyme protein kinase C (PKC).[21] Successively, the PMA can also activate the NF-κB-dependent transcription with negligible effects on the DNA binding. Furthermore, the extremely effective concentrations of both the TNFα and PMA can produce an improving effect on the NF-κB-dependent transcription.[22] Nonetheless, the superoxide radical was recognized as the major responsive oxygen species generated by the PMA in mouse macrophages.[23] In this context, the PMA has regularly been used as an inducer for endogenous superoxide productions,[24] and it has also been used to stimulate the B-cells divisions throughout the cytogenetic diagnosis of B-cell cancers, ie, chronic lymphocytic leukemia.[25] The nuclear factor kappa-B (NF-kB) family genes play vital roles in tumor growth, tissue development, metastasis, and decreased apoptosis.[26,27] Due to the inhibition of NF-kB, it can be taken as a potential pharmacological target for controlling the cancer progression, and further used in designing chemotherapeutic agents for oncological interventions through new drug discovery and improved chemotherapeutic regimes. This study aimed to establish the roles of the TNFα, and elaborate on the controls of the NF-κB activation in arresting the hallmarks of cancer in the backdrop of the presence of the freshly prepared AgNPs-CIT.

Materials and Methods
Materials
Silver nitrate (AgNO₃), tri-sodium citrate (TSC), sodium chloride, potassium chloride, disodium hydrogen phosphate, potassium dihydrogen phosphate, sodium hydroxide,

hydrogen peroxide, and hydrochloric acid, all chemicals were purchased from (VBBN company, Hong Kong, China). Phorbol 12-myristate 13-acetate (PMA), 2,2-diphenyl-1-picrylhydrazyl (DPPH) were purchased from Sigma-Aldrich (St. Louis, MO). Iscove's Modified Dulbecco's medium was purchased from Invitrogen (Carlsbad, CA), and iron-supplemented calf serum was procured from HyClone Laboratories (Logan, UT). Antibodies were purchased from Cell Signaling Technology Inc. (Danvers, MA), and Santa Cruz Biotechnology, Inc. (Santa Cruz, CA). NF-kB inhibitor (parthenolide) was purchased from Calbiochem (San Diego, CA). Kits for performing cytokine-specific enzyme-linked immunosorbent assays (ELISAs) were purchased from R&D Systems (St. Paul, MN). MCF-7 cell lines were purchased from the American Type Culture Collection (ATCC #ATCC® 30–4500K™, Middlesex, UK). All the chemicals were of analytical grades.

Methods
Synthesis of Silver Nanoparticles Using Trisodium Citrate
The AgNPs-CIT were prepared by the citrate reduction method following the previous reported method[28] with some modifications. Briefly, 8.5 mg of $AgNO_3$ was dissolved in 50 mL of Millipore-purified water to form a 1 mM stock solution (stock solution-I). The 6.8 mL of stock solution-I was diluted to 100 mL with Millipore water, and pH was adjusted to 8 using 10 mM NaOH solution. The Erlenmeyer flask containing the solution was stirred vigorously at $\approx$ 4000 rpm, and heated to 100 °C, wherein the temperature was adjusted using a mercury thermometer. The 2 mL of tri-sodium citrate (TSC) solution 38 mM (stock solution-II) was carefully added to the boiled solution in Erlenmeyer flask slowly and was let to continue boiling for another 15 min. The colorless so;ution was changed to yellow, pink, bright red, red, brown, and dark brown at 2, 4, 6, 8, 10, and 12 min respectively indicating the completion of the reaction after 12 min. The formed AgNPs-CIT had different colors from. The formed AgNPs-CIT were stored at room temperature in amber-color bottles. The particles were purified by centrifugation at 1000 rpm for 5 min to remove the large particulates.

UV-VIS Spectroscopy
The prepared AgNPs-CIT were synthesized at different time intervals, and each batch of the prepared NPs was recorded for the absorption spectra, and each preparation

had a specific UV spectrum according to their colors. Five absorption spectra for each preparation were recorded in the range from 300 to 700 nm on the Uvikon-941 spectrophotometer (Kontron Instruments GmbH, Herrenberg, Germany). The absorbance capacities of the samples were recorded in 2 cm path-length plastic cuvettes. The surface plasmon resonance (SPR) peaks were visible in the range and were drawn through excel Microsoft 2019,[29] provided as Figure 1.

Size and ζ-Potential Measurements by Dynamic Light Scattering (DLS) Instrument
The Malvern Zetasizer nano 6.01 (Malvern Instruments GmbH, Herrenberg, Germany) was used to measure the particle size, PDI, and the ζ-potential. The timing of sampling was automatically set on the instrument. For every 10 sub-runs, three measurements were permitted. All calculations were performed, according to the literature protocol in aqueous media.[29,30]

Surface Morphology Using Scanning Electron Microscopy (SEM) Analysis
SEM morphology was performed using a JEOL JSM-550 Scanning Electron Microscope (Jeol, Akishima, Tokyo, Japan) to analyze the superficial morphology of the prepared AgNPs-CIT. A drop of AgNPs-CIT was added on a slip-cover (Sputter coater, JOEL JFC-1300), was fully dried, and covered with a thin layer of platinum in a vacuum for 55 sec at 25 mÅ using a coating unit to make it electrically conductive before imaging in the SEM instrument.[31]

Fourier Transform Infrared (FT-IR) Spectroscopy
Fourier Transform Infrared (FT-IR) spectra of TSC, AgNPs-CIT, and $AgNO_3$ were recorded using (Bruker, OPTIK GmbH, Type: Tensor 27, Germany). The samples were scanned at the range of 400–4000 cm^{-1}. For purification of the prepared AgNPs-CIT, a solution of AgNPs-CIT was centrifuged at 12,500 rpm, for 20 min, and 3x washed with Millipore water. The dried powder was obtained after freeze-drying of the AgNPs-CIT sample was used for the FT-IR analysis.[29,30]

Radical Scavenging Activity
Diphenyl picrylhydrazyl (DPPH), and hydrogen peroxide (H_2O_2) were used to assay the scavenging activities of the AgNPs-CIT using the previously reported standard procedure.[32] In a typical experiment, about 2 mL of AgNPs-CIT solution was mixed with 2 mL of 0.1 mM DPPH solution in methanol and incubated at 37 °C in the
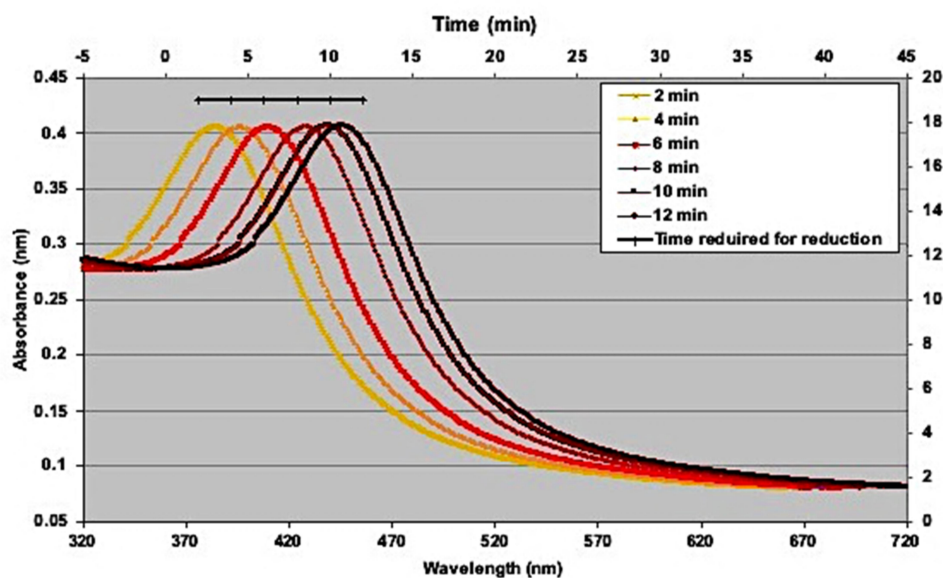
Figure 1 UV-VIS spectra of AgNPs-CIT reduced by TSC. The UV-VIS spectra of AgNPs-CIT showed a small redshift in the surface plasmon resonance peak for each NPs. Each peak represents the reduction with TSC at 2, 4, 6, 8, 10, and 12 min.

dark for about 40 min. The absorbance was recorded spectrophotometrically at 517 nm using methanol as the blank, while the H_2O_2 scavenging activity of AgNPs-CIT was measured through the reduction of H_2O_2. A 0.5 mL of AgNPs-CIT solution was added to 0.5 mL of 40 mM H_2O_2 which made up to 2 mL using 0.1 M phosphate buffer (pH 7.2), the mixture was incubated at 30 °C for 45 min. The absorbance was measured spectrophotometrically at 230 nm. The % DPPH/H_2O_2 radical scavenging activity was determined by the following equation:

$$\% \frac{DPPH}{H_2O_2} \text{ radical scavenging assay} = \frac{(A_0 - A_1)}{A_0} x100$$

Where, A_0 was the absorbance of the blank, and A_1 was the absorbance of the treated sample.

Cell Cultures

The MCF-7 cell-lines were grown as per their instructions (ATCC, VA, USA). Briefly, MCF-7 cell-lines were grown in RPMI-1640 medium supplemented with 10% heat-inactivated fetal bovine serum (FBS), and 1% penicillin-streptomycin at 37 °C in 5% CO2 as described.[33,34] The MCF-7 cell lines were cultured with PMA and AgNPs-CIT.

Treatment of MCF-7 Cell Lines with PMA and AgNPs-CIT

The PMA and AgNPs-CIT effects on the viability of the MCF-7 cell-lines were determined *invitro*. The MCF-7 cell-lines (1 × 106/mL) were placed in 35-mm culture dishes (Becton-Dickinson, Franklin Lakes, NJ, USA) in DMEM medium, or serum-starved for 12 hr/overnight. The MCF-7 cell-lines were cultured without PMA, or AgNPs-CIT served as controls. The cells were treated with various doses of AgNPs-CIT (0.5 to 160 μM) for 24–48 h of the incubation, and the cytotoxicity was examined using the CytoTox-Glo™, Cytotoxicity Assay Kit (Promega, Madison, WI, USA) as described.[35] In another set of experiments, MCF-7 cell-lines were pretreated with different doses of AgNPs-CIT (0.5–10 μM) for 2 h before its stimulation with PMA (0.5 μM) according to the reported procedure.[36,37]

Quantitative Real-Time PCR

Real-time quantitative PCR was used to quantify the expression of mRNA with GAPDH as endogenous control as described in earlier reports.[38,39] The total RNA was measured using a mirVana RNA isolation kit (catalog # AM1560; Ambion, Foster City, CA, USA) according to the manufacturer's instructions. Total RNA (1–2 μg) was reverse-transcribed using the SuperScript First-Strand cDNA synthesis kit (Applied Biosystems, Foster City, CA, USA). The expression of TNFα mRNA was quantified by TaqMan Gene Expression Assays (Applied Biosystems). Real-time PCR amplification and data capture were carried out using the Step One Real-Time PCR System (Applied Biosystems). Primers used for the PCR assisted

amplification were TNFα (NM_000595: forward, 5′-AGG ACG AAC ATC CAA CCT TCC CAA-3′; reverse, 5′-TTT GAG CCA GAA GAG GTT GAG GGT-3′), and GAPDH (NM_002046.3: forward, 5′-TCG ACA GTC AGC CGC ATC TTC TTT-3′; reverse, 5′-ACC AAA TCC GTT GAC TCC GAC CTT-3′). The typical profile times used were, with an initial step of 95 °C, for 10 min, followed by a second step, at 95 °C for 15 sec, and 60 °C for 60 sec for 40 cycles with melting curve analysis. The level of target mRNA was normalized to the level of GAPDH, and compared with control (untreated sample). Data were analyzed using the ΔΔCT method.[40]

TNFα ELISA

The MCF-7 cell-lines were pretreated with different doses of AgNPs-CIT (0.5–10 μM) for 2 h before stimulation with PMA (0.5 μM). The TNFα present in the culture medium was quantified using the TNFα-specific ELISA according to the manufacturer's instructions (R&D Systems, Minneapolis, MN, USA). ELISA kit (Cayman Chemicals, Ann Arbor, MI, USA) was used according to the instructions of the manufacturer, and the microtitre plate was read at 450 nm using an automatic microplate reader (Anthos Zenyth 3100 Multimode Detectors, Salzburg, Austria) as described in the literature.[41]

Nuclear Factor-Kappa-B Activity Assays

Inhibition of NF-κB p65 activity by AgNPs-CIT in PMA stimulated MCF-7 cell lines was determined using a highly sensitive Transcription Factor ELISA Kit according to the instructions of the manufacturer (catalog # ab133128, Abcam, MA, USA). The plate was read using an automatic microplate reader (Anthos Zenyth 3100 Multimode Detectors, Salzburg, Austria) according to the references.[42,43]

Results
UV-VIS Spectroscopy

During the experimental procedure upon the addition of TSC to AgNO$_3$, a color change was observed. The formed AgNPs-CIT were primarily yellowish, and upon further heatings, the color changed to pink, bright red, red, brown, and dark brown as the solution was kept boiling. The AgNPs-CIT generated the SPR absorption bands,[44] and the UV-VIS spectra of AgNPs-CIT showed a redshift in the SPR peaks for all of the produced different colors of AgNPs-CIT. The obtained colors had different wavelengths, for all the colors, ie, yellow, pink, bright red, red, brown, and dark brown at 2, 4, 6, 8, 10, and 12 min

with wavelengths of 381±1.6, 398±2, 413.5±1.5, 431±1.3, 440±3.5, and 452±1.5 nm, respectively (Figure 1).

Size, ζ-Potential, and Surface Morphology

The differential light scattering (DLS) instrument recorded the particle sizes of the AgNPs-CIT (Figure 2A) as being 19.2±0.1, 33.45±0.09, 67.77±0.1, 78.55±0.2, 120.67±0.11, and 220.77±0.12 nm for the yellow, pink, bright red, red, brown, and dark brown colored preparations, respectively, in agreement with the previously published results.[45] The ζ-potentials of AgNPs-CIT were negative surface charge values of −10.16±0.5, −14.63±0.6, −26.17±0.3, −34.63 ±0.1, −23.5±0.9, and −9.99±0.8 mV for yellow, pink, bright red, red, brown, and dark brown colored preparations, respectively (Figure 2B). The AgNPs-CIT had spherical shapes with an average diameter of 500 nm as shown by the SEM analyses (Figure 2C). All the PDIs values were below 0.2, representing a stable colloidal system for all the AgNPs-CIT preparations.

Fourier Transform Infrared (FT-IR) Spectroscopy

The surface functionalization of the prepared AgNPs-CIT, by the citrate moieties was confirmed from FT-IR analyses of the samples. The FT-IR spectral analysis confirmed the formation of the AgNPs-CIT, wherein it exhibited a strong absorption band for OH stretching at 3330 cm^{-1}. The hump-shaped absorption band at 1400 cm^{-1} in the AgNPs-CIT FT-IR spectrum, which is absent in the IR spectrum of the AgNO$_3$, resulting from the methylenes bending of the citrate moieties in the AgNPs-CIT preparations indicated the surface-bound citrates presence around the AgNPs.[46] The peak at 1610 cm^{-1} was attributed to (C=O) of the AgNPs-CIT (Figure 3).[47]

The Radical Scavenging Activity

The radical scavenging activity of AgNPs-CIT was confirmed against both the H$_2$O$_2$, and DPPH with quercetin as the reference standard (Figure 4). The AgNPs-CIT scavenged the free radicals at concentrations between 0.65–10 mg/mL. The data showed that the antioxidant activity of AgNPs-CIT was varying in comparison to that of H$_2$O$_2$ and quercetin from weak activity levels to moderate activity levels, wherein the best antioxidant activity of AgNPs-CIT was found at >40% (~ 42%) radicals inhibitions at 10 mg/mL concentration (Figure 4).[32,48]
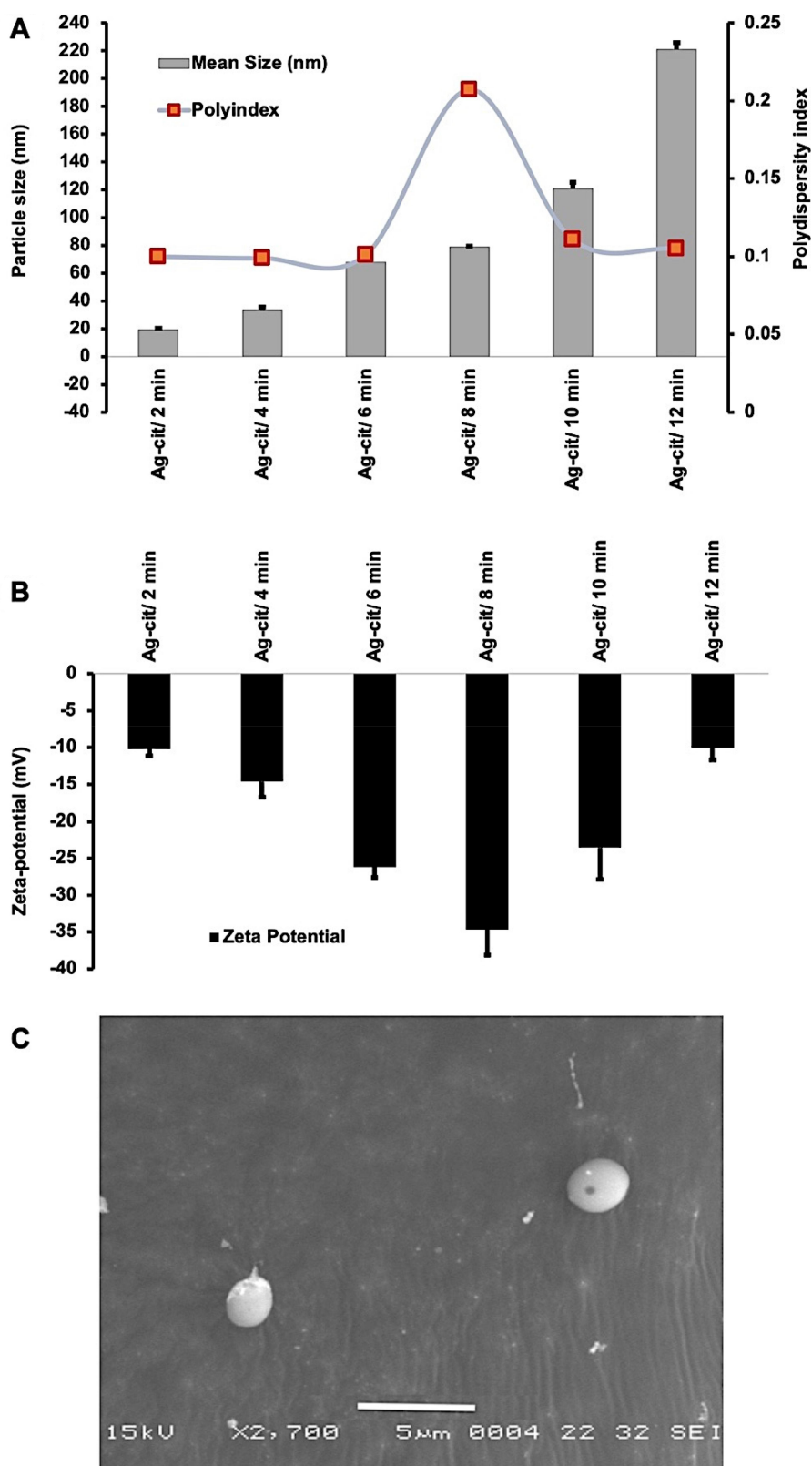
Figure 2 The size distribution of AgNPs-CIT; (**A**). The mean particle size (nm), (**B**). ζ-potentials (mV), and polydispersity indices of all AgNPs-CIT at 2, 4, 6, 8, 10, and 12 min; (**C**). SEM image of AgNPs-CIT reduced after 10 min.
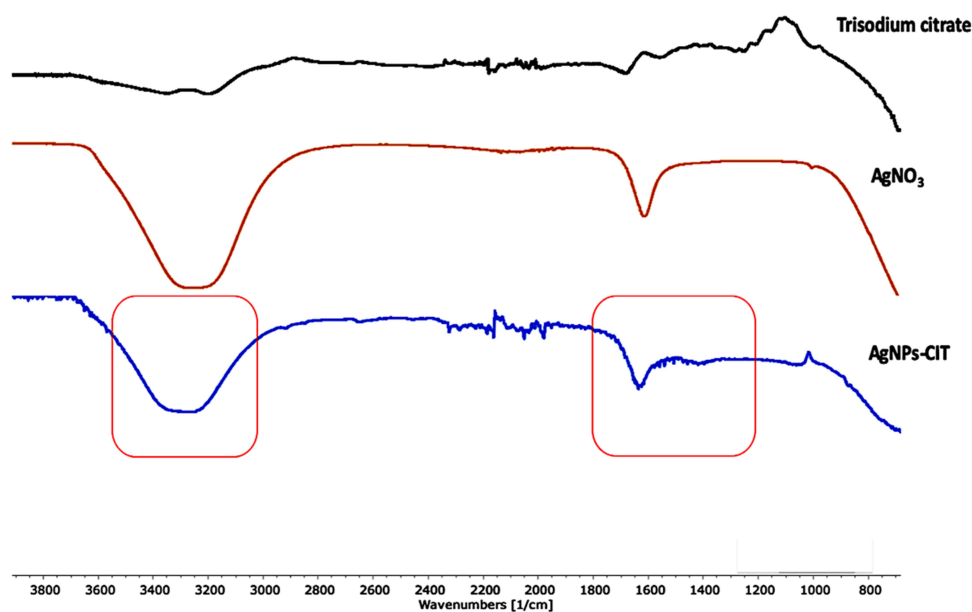
Figure 3 FT-IR spectra of silver nitrate (AgNO₃), AgNPs-CIT, and TSC. The black arrows represent the citrate area in TSC and AgNPs-CIT.
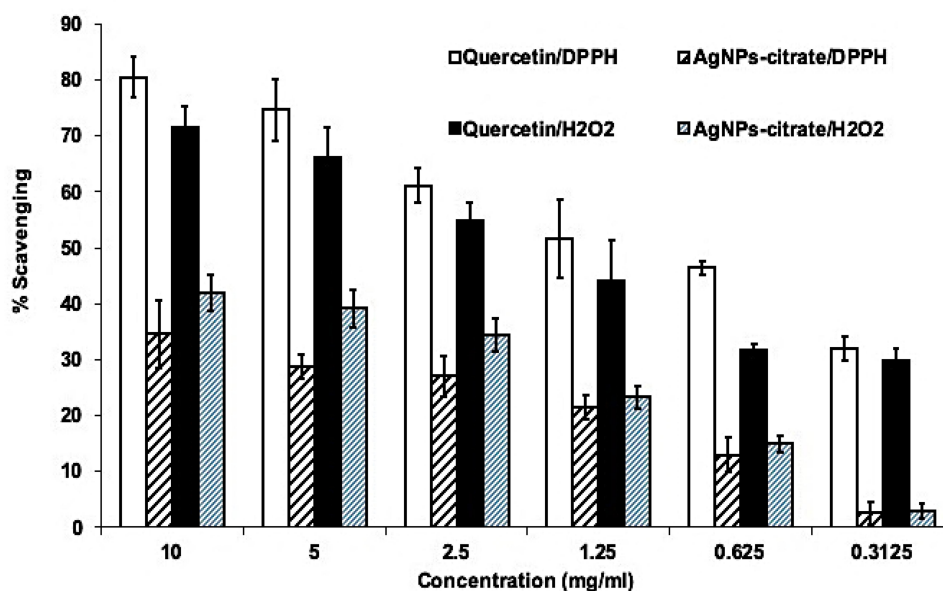

Figure 4 AgNPs-CIT radical scavenging (%) activity with DPPH, and hydrogen peroxide.

Treatment of MCF-7 with AgNPs-CIT

The AgNPs-CIT reduced at 8 min with a bright red coloration of the colloidal preparation having particle size at 78.55 ± 0.2 nm were selected for incubation with the MCF-7 cell-lines. The AgNPs-CIT utilized in incubation had ζ-potential at -34.63 ± 0.1 mV. This preparation had superior stability compared to the other preparations of the AgNPs-CIT because of its highest ζ-potential.[49] The cancer cell-lines, MCF-7, were pretreated with AgNPs-CIT (0.1–160

μM) for 2 h (Figure 5A), followed by stimulation with PMA (40 nM) for 24 h. The cytotoxicity of AgNPs-CIT on MCF-7 cell-lines after 24 h treatment was analyzed by using the CytoTox-Glo™-based cytotoxicity assay. The AgNPs-CIT cytotoxicities were checked using different concentrations of the AgNPs-CIT (0.1–160 μM). The higher concentration, 160 μM, of AgNPs-CIT was incubated with the MCF-7 cell-lines for different incubation times, from 4 to 48 h (Figure 5B), and it showed no
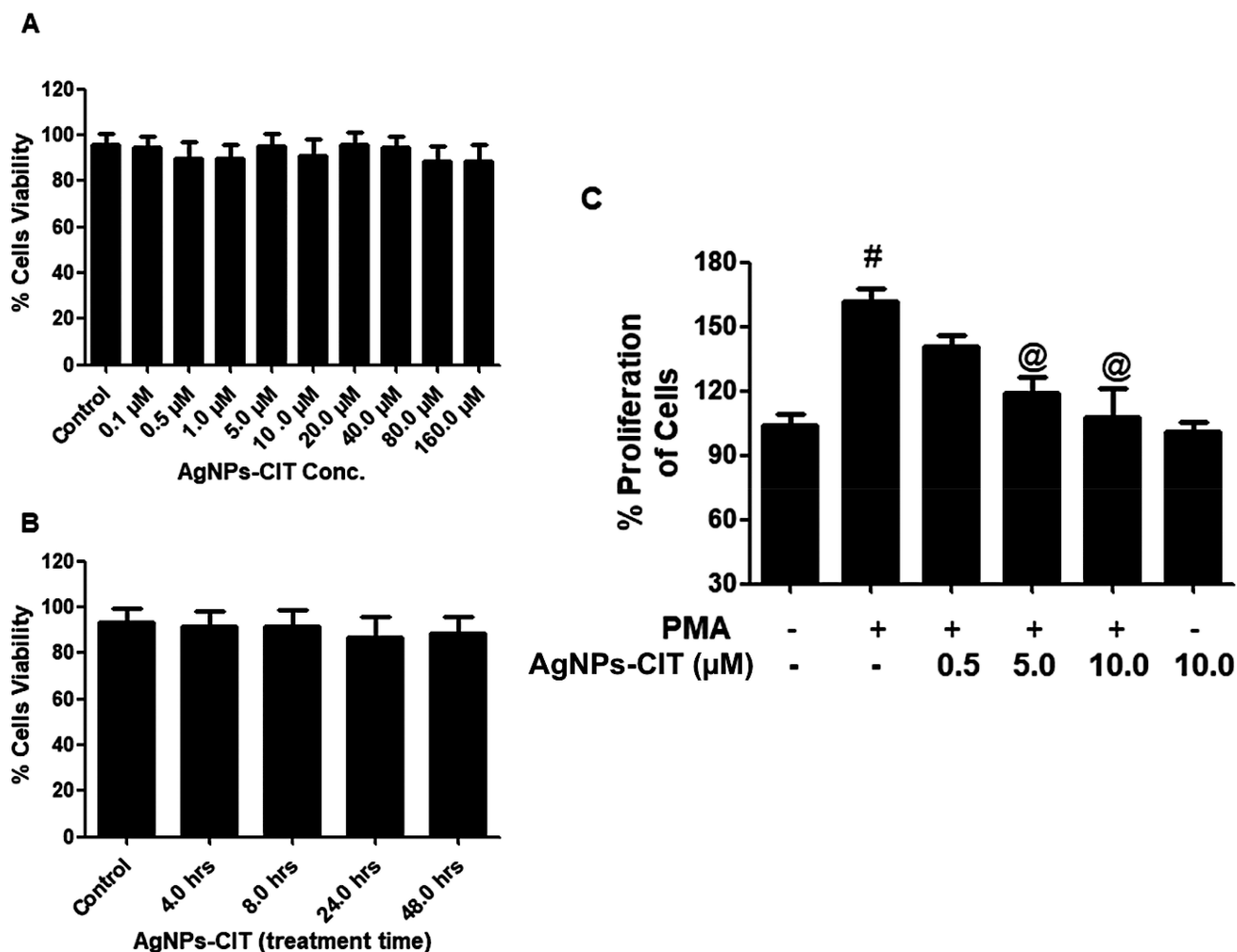
Figure 5 (**A**) Effects of AgNPs-CIT concentration (0.1–160 μM) on viability of MCF-7 cell lines. (**B**) Effects of AgNPs-CIT treatment time (4–48 hours) on viability of MCF-7 cell lines. (**C**) Effects of AgNPs-CIT on the proliferation of PMA-stimulated MCF-7 cell lines. MCF-7 cell lines were pretreated with AgNPs-CIT NP (0.5–10 μM) for 2 hours before stimulation with PMA (0.5 μM). #$p < 0.01$ versus untreated cells; @$p < 0.01$ versus PMA alone treated MCF-7 cells.

toxicity to the cells as determined by the MTT assay (Figure 5C).

The extent of cancer cell proliferation was significantly decreased when pretreated with AgNPs-CIT for 2 h and then stimulated with PMA for 24 h (Figure 5C; $p < 0.05$). The results showed that the pretreatment of breast cancer cell-lines with AgNPs-CIT significantly reduced the PMA-induced proliferation in a dose-dependent manner ($p < 0.05$).

The MCF-7 cell-lines pretreated with AgNPs-CIT (0.5 to 10 μM) for 2 h, followed by stimulation with PMA (0.5 μM) for 24 h, showed no cytotoxic effects of AgNPs-CIT at the levels of the administered dose ($p > 0.05$) (Figure 6A). The levels of TNFα mRNA were quantified by a highly sensitive, and specific quantitative RT-PCR method wherein the values were compared with the control. The results showed that the MCF-7 cell-lines incubated with PMA had higher levels of TNFα mRNA as compared to the unstimulated MCF-7 cell-lines ($p < 0.05$). The TNFα mRNA levels also showed a marked decline ($p < 0.01$). However, in the samples pretreated with PMA and incubated with AgNPs-CIT (Figure 6B), showed significant inhibition of TNFα mRNA, while at the same time showed of no effect because of PMA. To determine whether the inhibition of gene expression also affected the protein levels, the culture supernatants were assayed for TNFα protein using TNFα-specific ELISA. The pretreatment with 0.5 to 10 μM AgNPs-CIT significantly decreased the PMA-induced TNFα production in the culture supernatant of PMA-stimulated MCF-7 cell-lines ($p < 0.05$), thus establishing the roles of the PMA and the Ag-NPs-CIT in the process.

The nuclear factor, NF-κB, is a typical transcription factor involved in numerous inflammatory responses, and Bay-11-7082 (BAY) is a well-known inhibitor of its (NF-κB)
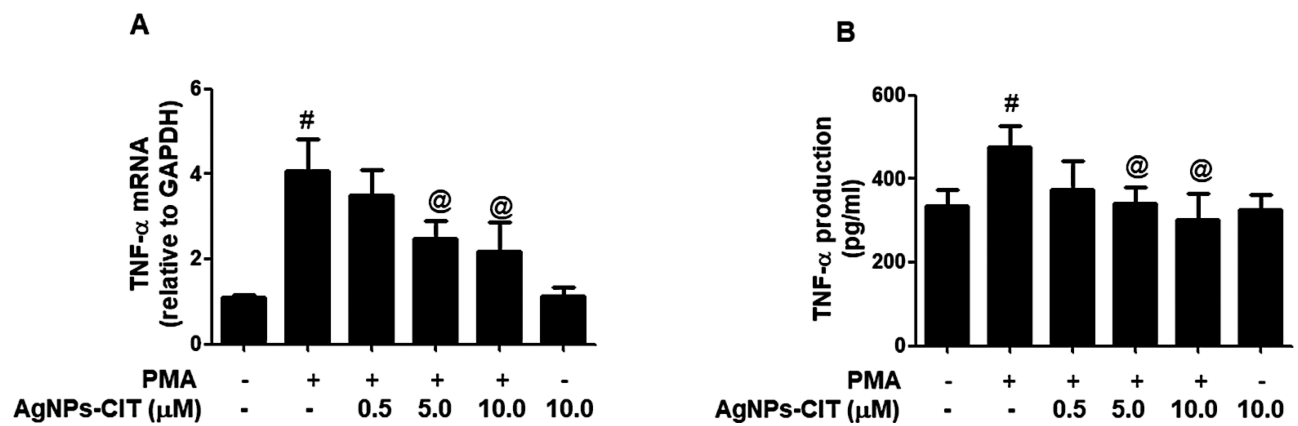
A

B

Figure 6 Gene and protein expression of TNFα. (**A**) Effect of AgNPs-CIT on PMA-induced gene expression of TNFα. Folds of TNFα mRNA expression as compared with control and normalized to GAPDH were determined by quantitative RT-PCR. (**B**) Effect of AgNPs-CIT on PMA-induced TNFα production in the culture medium of MCF-7 cell lines. The production level of TNFα was determined by sandwich ELISA. Results are representative (mean ± standard error of the mean) of triplicate experiments. #p<0.001 versus untreated MCF-7 cells; @p<0.01 versus PMA alone treated MCF-7 cells.

activity.[48] In the present study, BAY was used to study the effect of NF-κB activation in TNFα expression at both the genic and protein levels through observations in the MCF-7 cancer cell-lines under treatment with the AgNPs-CIT in presence of the PMA. The results showed that the treatment of cancer cell-lines with the BAY significantly reduced the mRNA (Figure 7A, p<0.05) and protein (Figure 7B, p<0.05)

levels of the TNFα in the PMA stimulated cancer cell-lines, clearly indicating the involvement of increased NF-κB activity in the PMA-induced expression of TNFα. Moreover, the involvement of NF-κB enhanced activity was further confirmed by the direct estimation of NF-κB levels in the nuclear extracts of MCF-7 cell-lines treated with the AgNPs-CIT and PMA. As shown in Figure 7C, the pretreatment of cancer
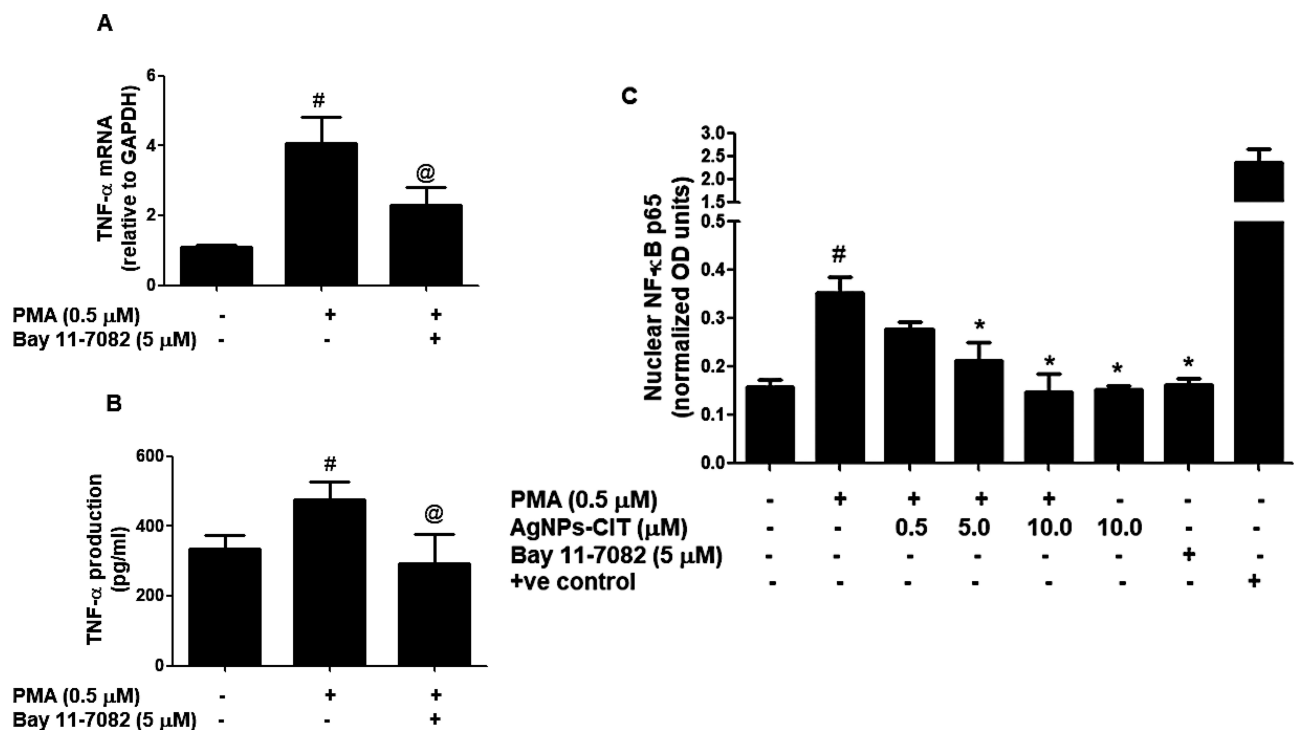
A

B

C

Figure 7 Effect of AgNPs-CIT and BAY on PMA-induced NF-κB pathway in MCF-7 cells. (**A**) Effect of BAY 11–7082 on PMA-induced TNF-α mRNA expression. #p<0.01 versus untreated MCF-7 cells, (**B**) Effect of BAY 11–7082 on PMA-induced TNF-α protein secretion in the culture medium of MCF-7 cells. @p<0.01 versus PMA alone treated MCF-7 cells, (**C**) Effect of AgNPs-CIT and BAY 11–7082 on PMA-induced NF-κB activation in the nuclear extract of MCF-7 cells. *p<0.05 versus PMA alone treated MCF-7 cells.

cell-lines with the increasing concentrations of AgNPs-CIT significantly decreased the PMA-induced nuclear NF-κB p65 levels (p<0.05) in the cancer cell-lines. The treatment of MCF-7 cell-lines with the BAY also significantly inhibited the NF-κB levels (p<0.01).

Discussion

The current study, for the first time, to the best of information, showed the AgNPs-CIT roles in inhibiting the PMA-induced TNFα production through deactivation of the NF-κB signaling events in the human breast cancer cell-lines, MCF-7. The AgNPs-CIT was synthesized (Figure 8) according to the known method with some modifications.[50]

The silver nitrate aqueous solution is reduced by the TSC to produce nano-seeds through the process of electrons combining with the silver ion. The formed nano-seeds combines together to produce the AgNPs-CIT which is hydrated around and covered with the citrate ions as part of the nanosilver stabilization, also represented as:

$AgNO_3$ + H_2O +$Na_3C_6H_5O_7$ →Ag^+ + e^- → Ag(NP seeds), Nucleation & Size growth + Stabilization → AgNPs-CIT

The FT-IR spectral analysis, together with electron micrography, confirmed the synthesis of AgNPs-CIT. In FT-IR analyses, a comparison showed peaks distinct from the TSC, $AgNO_3$, and AgNPs-CIT. The mechanistic pathway yielding the AgNPs-CIT was confirmed by the presence of OH, and C=O peaks of the citrate moieties and the hydration covering of the product which are absent in the reducing agent TSC, and the starting material, $AgNO_3$. The weak peak at 1400 cm^{-1} was also distinct for the product AgNPs-CIT and represented the methylenes bending of the citrate moieties which are exhibited in the TSC but are absent in the spectrum of $AgNO_3$. These peaks and their comparative analysis indicated the steps in the reaction mechanism of the preparation of the AgNPs-CIT as confirmed by the FT-IR

spectroscopy. The use of diluted silver ions concentration (mM range) as an aqueous solution of $AgNO_3$, lessens the chances of produced nano silver aggregation and helps to control the sizing of the NPs. Other factor, such as, the temperature and pH also play crucial roles in the formation, sizing, charge, and the polydispersity of the nano preparation.[51]

The UV-VIS spectroscopy, a measurement of the absorption characteristic of the prepared nano entities is part of the critical technique for confirmation of the preparation. The absorption wavelength is an indication of the size, reactivity, and the nature of the nano colloid.[52,53] The prepared AgNPs-CIT exhibited distinctive absorption peaks between 381–452 nm, indicating the excitation of the surface plasmon, presumably, owing to the presence of free electrons which generate the resonance of the SPR band.[44] The UV-VIS spectra of the AgNPs-CIT showed a gradual redshift, and the absorption peaks were attributed to the continuous increase in the sizes of the AgNPs-CIT overtime during the preparation. Steinigeweg et al[54] reported the synthesis of AgNPs-CIT, and therein the reaction was much faster as indicated by the rapid color changes of the reaction medium. The color changes were indicated by the changes in the absorption wavelengths of the nano preparations. Also, the maximum wavelength shifts of the absorption band occur due to the increase in the diameter of the nanospheroids.[55] Ranoszek-Soliwoda et al,[44] also observed the absorption band maxima (λ_{max}) at 432 nm when the synthesis was carried out at 100 °C, indicating the role of temperature in the synthesis and size-controls of the NPs. The size of the nanoparticle changes upon continuous energy supply to the reacting media, duration of the reaction, parameters of pH, variations in the concentrations of the reacting components as well as dilutions of the solvent/reacting media during the synthesis, the speed, and duration of the stirring/agitation which
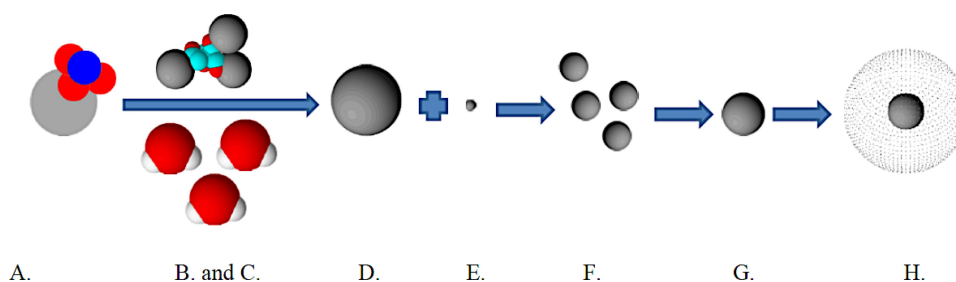

A. B. and C. D. E. F. G. H.

Figure 8 Schematic representation of the reaction mechanism of the silver nanoparticles formation: (A) Silver Nitrate ($AgNO_3$), (B). Tri-Sodium Citrate (TSC), (C). Water Molecules, (D). Silver ions, (E). Electron, (F). Nano-seeds (primitive nanoparticles). (G). Nucleation, aggregation of smaller nano-seeds, (H). Nanoparticle stabilization by citrate ions.

is also another source of energy than the heating of the reaction media (which may or may not be present in a particular synthesis), temperature maintenance and its up-scaling during the synthesis, intermolecular distances between the reacting components, formed nuclei, NPs, solvent molecules, and other components in the reacting pot, ie, presence of catalysts, biogenic materials from plants or other natural sources, synthetic entities as co-catalyst, and facilitators of the synthesis, present during the synthetic process. The morphology and charges on the nano preparation colloids are also variables through these parameters of change.[55]

During the current preparations, the particle sizes were observed to be increased which reflected the roles of various factors involved during the synthesis. The changes in the particle sizes were indicated by the color changes of the preparations, observed at different time intervals, ie, 2, 4, 6, 8, 10, and 12 min (Figure 1). The color changes of the preparations at different time intervals, the sizes of the NPs in the preparation at the specific time, and the UV-VIS absorption spectra of the colored solutions obtained at specific times were recorded and found to be between 381 and 452 nm range. Moreover, the nanoparticle sizing is also a function of the concentration of the reacting raw materials, and the silver ion source, ie, $AgNO_3$ concentration, as well as the presence and concentrations of the ionic molds, eg, citrate ions, as the anionic component in the aqueous medium, which also played the part in deciding the NPs sizes.[56] The relation between the size and color of the NPs was also reported by Fuku et al[45] who outlined that the colors of all plasmonic NPs can be altered by varying the size and morphology of the particles which is reflected in the changes in the SPR absorption wavelengths of the particles. The blue and redshifts in the absorptions are observed based on the reduction and increments in the NPs sizes.[45,56]

Moreover, the electronic images reflect the metallic center of the particles as they capture the core of the NPs after the surrounding hydrated area of the metal core (also containing citrate in AgNPs-CIT) is collapsed/removed during the sample preparation and image procurement processes for the electronic imaging, including the SEM high-vacuum chamber,[57] and is the reason behind the size differences with the other size measurement technique, ie, DLS technique. The sizes of the AgNPs-CIT NPs were recorded by the DLS and have shown the size difference owing to different techniques. Our interpretation is in agreement with the size recorded

with DLS, and the particle diameters from DLS are lower than those obtained from SEM imaging which is considered to be due to the presence of the citrate coating of the AgNPs-CIT, and this also limits the total particle density. The DLS estimates the average sizes of the NPs which are not the same and varies significantly from the sizes measured by the SEM technique. The DLS based average size estimations of the AgNPs-CIT suspension may also vary and at times may not be reproducible wherein the nanosuspension may aggregate and affect the average distribution of size.[58]

The presence of citrate anions frames in the preparation media works as scaffoldings that are adsorbed on the surfaces of the generating NPs. The prepared AgNPs-CIT were overwhelmingly negatively charged as observed in the ζ-potential measurements. Their charges varied from -9.99 ± 0.8 to -34.63 ± 0.1 mV with changes in size and colors. The high negative ζ-potential of the red-colored AgNPs-CIT indicated that the particles are of the highest electrically stabilized nature to resist aggregation. Similar results were also reported by Greenwood et al,[59] and Moraes et al,[60] who reported that the size, PDI, and ζ-potential are parameters that indicate the stability of NPs. Kaufman et al,[49] stated that the surface charges upon NPs play significant roles in the stabilization of the NPs, whereas the degrees of ζ-potential is a parameter of the colloidal stability of the system. The PDI, considered as an indication of the near homogeneity of the particles' sizes in the sample of the NPs, are interpreted as, if the PDIs is lower than 0.2, the particle size distribution falls within a narrow range of sizes,[61] and is considered ideal. Also, there are particles aggregation and size increase which leads to a reduction in ζ-potentials of the last two samples (-23.5 ± 0.9, and -9.99 ± 0.8 mV) obtained at 10 and 12 min of the preparation with higher sizes (120.67 ± 0.11, and 220.77 ± 0.12 nm, DLS), and high UV-VIS absorbance values at 440 ± 3.5, and 452 ± 1.5 nm, respectively. These results are in agreement with Guang Lu et al observations on the ζ-potential values that explained that distinct stability can be expected around $(+10)-(-10)$ mV ζ-potential values. Other considerations, such as reduced size have also played a significant role in stabilizing the NPs.[62]

The antioxidants are useful in quenching and minimizing the effects of excessively generated free radicals in the human body which can destroy the cell components, cause permanent cell damages, and eventual cell death. It plays havoc with the lipids, proteins, and DNA, leading to cancers and other diseases. The antioxidant activity

evaluation of the AgNPs-CIT showed noticeable anti oxidant activity at about 40% inhibitions of the DPPH radicals when compared with the hydrogen peroxide and quercetin (Figure 4). The antioxidant activity of AgNPs-CIT was attributed to the surface-presence of the citrate molds on the AgNPs-CIT.[63] Akhtar et al[48] concluded that the antioxidant efficacy of AgNPs could be acknowledged to the probable adsorption of coating layer around AgNPs of various phytochemicals e.g; polyphenols, flavonoids, saponins, terpenoids, and vitamins which is the cause of strong antioxidant activity of the phytochemicals supported NPs synthesis. In the case of the present synthesis, the moderate antioxidant activity is due to the presence of citrate moieties around the AgNPs.

The AgNPs-CIT showed no toxicity to the breast cancer cell-lines, MCF-7, as determined by CytoTox-Glo™ Cytotoxicity assays. The concentrations used in these assays were in conformity with the procedure and results reported by Yingying et al.[5] The cytotoxicity evaluations showed that cell proliferation of MCF-7 cell-lines, after treatment with AgNPs-CIT, was termination as observed in the incubation of MCF-7 cell-lines with AgNPs-CIT for 24 and 48 h. The extent of PMA-induced proliferation was significantly decreased when the MCF-7 cell-lines were first treated with AgNPs-CIT. The cells pretreated with 5 and 10 µM doses of AgNPs-CIT for 48 h highlighted the proliferation of AgNPs-CIT treated MCF-7 cell lines. Importantly, no cytotoxic effects of AgNPs-CIT were observed at the levels of the administered dose. Moreover, the levels of TNFα mRNA production were assayed by the quantitative RT-PCR method, and the results showed that the MCF-7 cell-lines incubated with PMA had higher levels of TNFα mRNA as compared to the non-stimulated MCF-7 cell-lines. The TNFα mRNA levels showed a marked decline.

The activation of the master transcription factor, NF-κB, leads to coordinated expression of many genes that encode cytokines, chemokines, enzymes, and adhesion molecules involved in mediator synthesis, and further amplification and perpetuation of the inflammatory reactions.[37] The expression of the TNF-α gene is dependent on the activation of transcription factor NF-κB.[41] Because the suppression of NF-κB activation has been linked with anti-inflammatory activity, it was postulated that the silver ions from AgNPs-CIT mediate its inhibitory effects on TNFα expressions, at least in part, through the suppression of the NF-κB activity. The activation of NF-κB requires proteolytic degradation of the inhibitory protein IκBα, an endogenous inhibitor, that binds to NF-κB in the cytoplasm, and its degradation exposes the nuclear localization signal and allows the NF-κB to translocate to the nucleus and binds with the promoter of the target genes.[37,41] In PMA-stimulated MCF-7 cell-lines, the AgNPs-CIT inhibit the nuclear translocation of the p65 NF-κB. These results were further confirmed by the treatment of cancer cell-lines with BAY-11, a well-known inhibitor of NF-κB activity.[39] These data indicate that the AgNPs-CIT significantly decreased the PMA stimulated inflammatory gene expression and production of TNF-α in MCF-7 breast cancer cell-lines. The inhibitory effect of silver nanoparticles on the pro-inflammatory cytokine, TNF-α, was NF-κB dependent. The inhibitory effects of the AgNPs-CIT on MCF-7 cell-lines differentiation at higher doses was attributed to the increased concentrations of the AgNPs-CIT.

Conclusions

The synthesized AgNPs-CIT were characterized through physicochemical methods, and the antioxidant assays of the NPs showed moderate levels of reactive oxygen species radical scavenging activity of the DPPH against the quercetin. The synthesized AgNPs-CIT were sufficiently stable in the physiological conditions to demonstrate its bioactivity in the designated activity environment. The AgNP-CIT worked as an inhibitor of PMA-induced activation of NF-κB signalings as well as an inhibitor of the TNF-α productions at significant levels which corroborated the hypothesis on the cancer suppression through signaling manipulation by physiological and biochemical means and pathways. Observations also confirmed the roles of the physiological pathways in the tumor progression and provided a confirmatory route to suppress the tumor growth through cutting-short the signaling pathway. These findings upload significant future roles in finding new clinical entities and approaches for cancer prevention and treatments. The study may also provide an alternative strategy for further adjudication of AgNPs-CIT as part of a chemotherapeutic regimen for TNF-α produced breast cancer's safe and potent treatment.

Research on Human Participants and/or Animals

No research was conducted on human participants or animals for this study.

Funding

the financial support for this research under the number (5551-pharmacy-2019-2-2-I) during the academic years 1440 AH/2019 AD.

Disclosure

The authors declare no conflict of interest.

References

1. Bastús NG, Merkoçi F, Piella J, Puntes V. Synthesis of highly monodisperse citrate-stabilized silver nanoparticles of up to 200 nm: kinetic control and catalytic properties. *Chem Mater*. 2014;26 (9):2836–2846. doi:10.1021/cm500316k

2. Yang Y, Xu S, Xu G, et al. Effects of ionic strength on physicochemical properties and toxicity of silver nanoparticles. *Sci Total Environ*. 2019;647:1088–1096. doi:10.1016/j.scitotenv.2018.08.064

3. Kavuličová J, Mražíková A, Velgosová O, Ivánová D, Kubovčíková M. Stability of synthesized silver nanoparticles in citrate and mixed gelatin/citrate solution. *Acta Polytech*. 2018;58 (2):104. doi:10.14311/AP.2018.58.0104

4. Benn TM, Westerhoff P. Nanoparticle silver released into water from commercially available sock fabrics. *Environ Sci Technol*. 2008;42 (11):4133–4139. doi:10.1021/es7032718

5. Xu Y, Wang L, Bai R, Zhang T, Chen C. Silver nanoparticles impede phorbol myristate acetate-induced monocyte-macrophage differentiation and autophagy. *Nanoscale*. 2015;7(38):16100–16109.

6. Sriram MI, Kanth SB, Kalishwaralal K, Gurunathan S. Antitumor activity of silver nanoparticles in Dalton's lymphoma ascites tumor model. *Int J Nanomedicine*. 2010;5:753–762.

7. Dowlati Y, Herrmann N, Swardfager W, et al. A meta-analysis of cytokines in major depression. *Biol Psychiatry*. 2010;67(5):446–457. doi:10.1016/j.biopsych.2009.09.033

8. Swardfager W, Lanctot K, Rothenburg L, Wong A, Cappell J, Herrmann N. A meta-analysis of cytokines in Alzheimer's disease. *Biol Psychiatry*. 2010;68(10):930–941. doi:10.1016/j.biopsych.2010.06.012

9. Locksley RM, Killeen N, Lenardo MJ. The TNF and TNF receptor superfamilies: integrating mammalian biology. *Cell*. 2001;104 (4):487–501. doi:10.1016/S0092-8674(01)00237-9

10. Bobinska K, Galecka E, Szemraj J, Galecki P, Talarowska M. Is there a link between TNF gene expression and cognitive deficits in depression? *Acta Biochim Pol*. 2017;64(1):65–73.

11. Tracey KJ, Fong Y, Hesse DG, et al. Anti-cachectin/TNF monoclonal antibodies prevent septic shock during lethal bacteraemia. *Nature*. 1987;330(6149):662–664. doi:10.1038/330662a0

12. Saha RN, Pahan K. Tumor necrosis factor-alpha at the crossroads of neuronal life and death during HIV-associated dementia. *J Neurochem*. 2003;86(5):1057–1071.

13. Zhou XL, Fan W, Yang G, Yu MX. The clinical significance of PR, ER, NF- kappa B, and TNF- alpha in breast cancer. *Dis Markers*. 2014;2014:494581. doi:10.1155/2014/494581

14. Ma J, Zhang Z, Zhang L. Expression of NF-kappa B and AP-1 in non-small cell lung cancer. *Zhongguo Fei Ai Za Zhi*. 2005;8 (5):440–443.

15. Deng J, Miller SA, Wang HY, et al. Beta-catenin interacts with and inhibits NF-kappa B in human colon and breast cancer. *Cancer Cell*. 2002;2(4):323–334. doi:10.1016/S1535-6108(02)00154-X

16. Rosales C, Juliano R. Integrin signaling to NF-kappa B in monocytic leukemia cells is blocked by activated oncogenes. *Cancer Res*. 1996;56(10):2302–2305.

17. Cai D, Yuan M, Frantz DF, et al. Local and systemic insulin resistance resulting from hepatic activation of IKK-beta and NF-kappaB. *Nat Med*. 2005;11(2):183–190. doi:10.1038/nm1166

18. Korkaya H, Liu S, Wicha MS. Breast cancer stem cells, cytokine networks, and the tumor microenvironment. *J Clin Invest*. 2011;121 (10):3804–3809. doi:10.1172/JCI57099

19. Perrot-Applanat M, Vacher S, Toullec A, et al. Similar NF-kappaB gene signatures in TNF-alpha treated human endothelial cells and breast tumor biopsies. *PLoS One*. 2011;6(7):e21589. doi:10.1371/journal.pone.0021589

20. Ben-Baruch A. Host microenvironment in breast cancer development: inflammatory cells, cytokines and chemokines in breast cancer progression: reciprocal tumor–microenvironment interactions. *Breast Cancer Res*. 2002;5(1):31–36. doi:10.1186/bcr554

21. Blumberg PM. Protein kinase C as the receptor for the phorbol ester tumor promoters: sixth Rhoads memorial award lecture. *Cancer Res*. 1988;48(1):1–8.

22. Holden NS, Squires PE, Kaur M, Bland R, Jones CE, Newton R. Phorbol ester-stimulated NF-kappaB-dependent transcription: roles for isoforms of novel protein kinase C. *Cell Signal*. 2008;20 (7):1338–1348. doi:10.1016/j.cellsig.2008.03.001

23. Swindle EJ, Hunt JA, Coleman JW. A comparison of reactive oxygen species generation by rat peritoneal macrophages and mast cells using the highly sensitive real-time chemiluminescent probe pholasin: inhibition of antigen-induced mast cell degranulation by macrophage-derived hydrogen peroxide. *J Immunol*. 2002;169(10):5866–5873.

24. Huang R, Zhao L, Chen H, et al. Megakaryocytic differentiation of K562 cells induced by PMA reduced the activity of respiratory chain complex IV. *PLoS One*. 2014;9(5):e96246. doi:10.1371/journal.pone.0096246

25. Arsham MS, Barch MJ, Lawce HJ. *The AGT Cytogenetics Laboratory Manual*. 2017.

26. Wulczyn FG, Krappmann D, Scheidereit C. The NF-kappa B/Rel and I kappa B gene families: mediators of immune response and inflammation. *J Mol Med (Berl)*. 1996;74(12):749–769. doi:10.1007/s001090050078

27. Pallares J, Martinez-Guitarte JL, Dolcet X, et al. Abnormalities in the NF-kappaB family and related proteins in endometrial carcinoma. *J Pathol*. 2004;204(5):569–577. doi:10.1002/path.1666

28. Romer I, White TA, Baalousha M, Chipman K, Viant MR, Lead JR. Aggregation and dispersion of silver nanoparticles in exposure media for aquatic toxicity tests. *J Chromatogr A*. 2011;1218 (27):4226–4233. doi:10.1016/j.chroma.2011.03.034

29. Abdellatif AA, Zayed G, El-Bakry A, Zaky A, Saleem IY, Tawfeek HM. Novel gold nanoparticles coated with somatostatin as a potential delivery system for targeting somatostatin receptors. *Drug Dev Ind Pharm*. 2016;42(11):1782–1791. doi:10.3109/03639045.2016.1173052

30. Abdellatif AAH, El Hamd MA, Salman KH, Abd-El-Rahim AM, El-Maghrabey M, Tawfeek HM. Integrative physicochemical and HPLC assessment studies for the inclusion of lornoxicam in buffalo's milk fat globules as a potential carrier delivery system for lipophilic drugs. *Microchem J*. 2020;152.

31. Patel N, Lalwani D, Gollmer S, Injeti E, Sari Y, Nesamony J. Development and evaluation of a calcium alginate based oral ceftriaxone sodium formulation. *Prog Biomater*. 2016;5(2):117–133. doi:10.1007/s40204-016-0051-9

32. Ali BM, Boothapandi M, Sultan Nasar A. Nitric oxide, DPPH and hydrogen peroxide radical scavenging activity of TEMPO terminated polyurethane dendrimers: data supporting antioxidant activity of radical dendrimers. *Data Brief*. 2020;28:104972. doi:10.1016/j.dib.2019.104972

33. Rasheed Z, Rasheed N, Abdulmonem WA, Khan MI. MicroRNA-125b-5p regulates IL-1beta induced inflammatory genes via targeting TRAF6-mediated MAPKs and NF-kappaB signaling in human osteoarthritic chondrocytes. *Sci Rep*. 2019;9(1):6882. doi:10.1038/s41598-019-42601-3

34. Rasheed Z, Al-Shobaili HA, Rasheed N, Mahmood A, Khan MI. MicroRNA-26a-5p regulates the expression of inducible nitric oxide synthase via activation of NF-kappaB pathway in human osteoarthritis chondrocytes. *Arch Biochem Biophys*. 2016;594:61–67. doi:10.1016/j.abb.2016.02.003

35. Rasheed Z, Rasheed N, Al-Shaya O. Epigallocatechin-3-O-gallate modulates global microRNA expression in interleukin-1beta-stimulated human osteoarthritis chondrocytes: potential role of EGCG on negative co-regulation of microRNA-140-3p and ADAMTS5. *Eur J Nutr*. 2018;57(3):917–928. doi:10.1007/s00394-016-1375-x

36. Rasheed Z, Rasheed N, Al-Shobaili HA. Epigallocatechin-3-O-gallate up-regulates microRNA-199a-3p expression by down-regulating the expression of cyclooxygenase-2 in stimulated human osteoarthritis chondrocytes. *J Cell Mol Med*. 2016;20 (12):2241–2248. doi:10.1111/jcmm.12897

37. Rasheed Z, Akhtar N, Anbazhagan AN, Ramamurthy S, Shukla M, Haqqi TM. Polyphenol-rich pomegranate fruit extract (POMx) suppresses PMACI-induced expression of pro-inflammatory cytokines by inhibiting the activation of MAP Kinases and NF-kappaB in human KU812 cells. *J Inflamm (Lond)*. 2009;6(1):1. doi:10.1186/1476-9255-6-1

38. Rasheed Z, Al-Shobaili HA, Rasheed N, et al. Integrated study of globally expressed microRNAs in IL-1beta-stimulated human osteoarthritis chondrocytes and osteoarthritis relevant genes: a microarray and bioinformatics analysis. *Nucleosides Nucleotides Nucleic Acids*. 2016;35(7):335–355. doi:10.1080/15257770.2016.1163380

39. Rasheed Z, Haqqi TM. Endoplasmic reticulum stress induces the expression of COX-2 through activation of eIF2alpha, p38-MAPK and NF-kappaB in advanced glycation end products stimulated human chondrocytes. *Biochim Biophys Acta*. 2012;1823 (12):2179–2189. doi:10.1016/j.bbamcr.2012.08.021

40. Pfaffl MW. A new mathematical model for relative quantification in real-time RT-PCR. *Nucleic Acids Res*. 2001;29(9):e45. doi:10.1093/nar/29.9.e45

41. Rasheed Z, Akhtar N, Khan A, Khan KA, Haqqi TM. Butrin, isobutrin, and butein from medicinal plant Butea monosperma selectively inhibit nuclear factor-kappaB in activated human mast cells: suppression of tumor necrosis factor-alpha, interleukin (IL)-6, and IL-8. *J Pharmacol Exp Ther*. 2010;333(2):354–363. doi:10.1124/jpet.109.165209

42. Rasheed N, Alghasham A, Rasheed Z. Lactoferrin from camelus dromedarius inhibits nuclear transcription factor-kappa b activation, cyclooxygenase-2 expression and prostaglandin e2 production in stimulated human chondrocytes. *Pharmacognosy Res*. 2016;8 (2):135–141. doi:10.4103/0974-8490.175612

43. Rasheed Z, Anbazhagan AN, Akhtar N, Ramamurthy S, Voss FR, Haqqi TM. Green tea polyphenol epigallocatechin-3-gallate inhibits advanced glycation end product-induced expression of tumor necrosis factor-alpha and matrix metalloproteinase-13 in human chondrocytes. *Arthritis Res Ther*. 2009;11(3):R71. doi:10.1186/ar2700

44. Ranoszek-Soliwoda K, Tomaszewska E, Socha E, et al. The role of tannic acid and sodium citrate in the synthesis of silver nanoparticles. *J Nanopart Res*. 2017;19(8):273. doi:10.1007/s11051-017-3973-9

45. Fuku K, Hayashi R, Takakura S, Kamegawa T, Mori K, Yamashita H. The synthesis of size- and color-controlled silver nanoparticles by using microwave heating and their enhanced catalytic activity by localized surface plasmon resonance. *Angew Chem Int Ed Engl*. 2013;52(29):7446–7450. doi:10.1002/anie.201301652

46. Munro CH, Smith WE, Garner M, Clarkson J, White PC. Characterization of the surface of a citrate-reduced colloid optimized for use as a substrate for surface-enhanced resonance raman scattering. *Langmuir*. 1995;11(10):3712–3720. doi:10.1021/la00010a021

47. Marcilla A, Gomez-Siurana A, Beltran M, Martinez-Castellanos I, Blasco I, Berenguer D. TGA-FTIR study of the pyrolysis of sodium citrate and its effect on the pyrolysis of tobacco and tobacco/SBA-15 mixtures under N2 and air atmospheres. *J Sci Food Agric*. 2018;98 (15):5916–5931. doi:10.1002/jsfa.9121

48. Akhtar MS, Swamy MK, Umar A, Al Sahli AA. Biosynthesis and characterization of silver nanoparticles from methanol leaf extract of cassia didymobotrya and assessment of their antioxidant and antibacterial activities. *J Nanosci Nanotechnol*. 2015;15(12):9818–9823. doi:10.1166/jnn.2015.10966

49. Kaufman ED, Belyea J, Johnson MC, et al. Probing protein adsorption onto mercaptoundecanoic acid stabilized gold nanoparticles and surfaces by quartz crystal microbalance and zeta-potential measurements. *Langmuir*. 2007;23(11):6053–6062. doi:10.1021/la063725a

50. Afshinnia K, Baalousha M. Effect of phosphate buffer on aggregation kinetics of citrate-coated silver nanoparticles induced by monovalent and divalent electrolytes. *Sci Total Environ*. 2017;581–582:268–276. doi:10.1016/j.scitotenv.2016.12.117

51. Abdellatif AAH, Tawfeek HM. Development and evaluation of fluorescent gold nanoparticles. *Drug Dev Ind Pharm*. 2018;44 (10):1679–1684. doi:10.1080/03639045.2018.1483400

52. Abdellatif AAH. A plausible way for excretion of metal nanoparticles via active targeting. *Drug Dev Ind Pharm*. 2020;46(5):744–750. doi:10.1080/03639045.2020.1752710

53. Abdellatif AAH, Abou-Taleb HA, Abd El Ghany AA, Lutz I, Bouazzaoui A. Targeting of somatostatin receptors expressed in blood cells using quantum dots coated with vapreotide. *Saudi Pharm J*. 2018;26(8):1162–1169. doi:10.1016/j.jsps.2018.07.004

54. Steinigeweg D, Schlucker S. Monodispersity and size control in the synthesis of 20–100 nm quasi-spherical silver nanoparticles by citrate and ascorbic acid reduction in glycerol-water mixtures. *Chem Commun (Camb)*. 2012;48(69):8682–8684. doi:10.1039/c2cc33850e

55. Abdellatif AAH, Ibrahim MA, Amin MA, et al. Cetuximab conjugated with octreotide and entrapped calcium alginate-beads for targeting somatostatin receptors. *Sci Rep*. 2020;10(1):4736. doi:10.1038/s41598-020-61605-y

56. Shirahata N, Hirakawa D, Masuda Y, Sakka Y. Size-dependent color tuning of efficiently luminescent germanium nanoparticles. *Langmuir*. 2013;29(24):7401–7410. doi:10.1021/la303482s

57. Fissan H, Ristig S, Kaminski H, Asbach C, Epple M. Comparison of different characterization methods for nanoparticle dispersions before and after aerosolization. *Anal Methods*. 2014;6(18):18. doi:10.1039/C4AY01203H

58. Zheng T, Bott S, Huo Q. Techniques for accurate sizing of gold nanoparticles using dynamic light scattering with particular application to chemical and biological sensing based on aggregate formation. *ACS Appl Mater Interfaces*. 2016;8(33):21585–21594. doi:10.1021/acsami.6b06903

59. Greenwood R, Kendall K. Selection of suitable dispersants for aqueous suspensions of zirconia and titania powders using acoustophoresis. *J Eur Ceram Soc*. 1999;19(4):479–488. doi:10.1016/S0955-2219(98)00208-8

60. Moraes CM, De Paula E, Rosa AH, Fraceto LF. Physicochemical stability of poly(lactide-co-glycolide) nanocapsules containing the local anesthetic bupivacaine. *J Braz Chem Soc*. 2010;21 (6):995–1000. doi:10.1590/S0103-50532010000600008

61. Vieville J, Tanty M, Delsuc MA. Polydispersity index of polymers revealed by DOSY NMR. *J Magn Reson*. 2011;212(1):169–173. doi:10.1016/j.jmr.2011.06.020

62. Lu GW, Gao P. Emulsions and microemulsions for topical and transdermal drug delivery. In: *Handbook of Non-Invasive Drug Delivery Systems*. 2010:59–94.

63. Sallam KI. Antimicrobial and antioxidant effects of sodium acetate, sodium lactate, and sodium citrate in refrigerated sliced salmon. *Food Control*. 2007;18(5):566–575. doi:10.1016/j.foodcont.2006.02.002